

Lattice Boltzmann simulations of conjugate heat transfer in high-frequency oscillating flows

Fankong Meng^a, Moran Wang^b, Zhixin Li^{a,*}

^a Department of Engineering Mechanics, Tsinghua University, Beijing 100084, China

^b Department of Biological and Agriculture Engineering, University of California, Davis, CA 95616, USA

ARTICLE INFO

Article history:

Received 20 March 2007

Received in revised form 22 January 2008

Accepted 4 March 2008

Available online 22 April 2008

Keywords:

Lattice Boltzmann method

Conjugate heat transfer

Oscillating flow

Acoustic streaming

ABSTRACT

The thermal lattice Boltzmann method (LBM) is used to simulate the conjugate heat transfer of high-frequency oscillating flows between two flat plates with different outer surface temperatures. The thermal boundary condition at the fluid–solid interface assumes that the unknown energy distribution functions of the fluid and the solid are in equilibrium with the counter-slip internal energy. The counter-slip internal energy was determined by constraints in the continuities of temperature and heat flux at the solid–fluid interface. Velocity, temperature and heat flux distributions are presented for various Stokes numbers, pressure oscillation amplitudes and plate to fluid thermal conductivity ratios. For relatively low-frequency oscillations (30 kHz) and small pressure amplitudes, the periodically averaged heat fluxes of the oscillating flow are almost equal to those of pure heat conduction. The averaged heat flux of the oscillating flow decreases with increasing pressure amplitudes and are less than those of pure heat conduction for relatively low frequencies (30 kHz) and large pressure amplitude oscillations. For high-frequency oscillations, the heat transfer is enhanced markedly by nonlinear acoustic streaming, where the average velocity rapidly increases with frequency.

© 2008 Elsevier Inc. All rights reserved.

1. Introduction

Conjugate heat transfer occurs when a fluid flows along a conducting solid wall with finite thickness. The behavior of the conjugate interface temperature or heat flux along the flow path cannot be prescribed as it depends on the flow properties, the flow dynamics and the wall properties. The simplest boundary conditions, such as constant wall temperature or constant heat flux, are not suitable because heat conduction in the solids also plays an important role in the overall heat transfer. Conjugate heat transfer is involved in many practical applications, such as thermoacoustic engines (Swift, 1988; Backhaus and Swift, 1999; Nika et al., 2005), MEMS (Fedorov and Viskanta, 2000; Li et al., 2004), the cooling of turbine blades (Mazur et al., 2006) and in the cooling of electronics (Horvat and Catton, 2003). Thermoacoustic engines utilize the interaction between an oscillating gas and a porous solid possessing a temperature gradient to convert heat to useful acoustic power, or to pump heat from low to high temperature regions while consuming acoustic power (Swift, 1988). Thermoacoustic engines have many advantages, such as no moving parts for the thermodynamic cycle, reliability and long life span with environmentally friendly inert gases used as the working medium. Ther-

moacoustic engines have been rapidly developed in recent years. The conjugate heat transfer of an oscillating flow is a typical phenomenon in thermoacoustic engines (Nika et al., 2005). To understand the thermoacoustic effect and to improve the performance of thermoacoustic engines, the characteristics of the conjugate heat transfer of oscillating flows should be clearly understood. High-frequency oscillating flows frequencies of up to thousands of Hertz may be used for microscale thermoacoustic engines (Chen et al., 2002; Symko et al., 2004) which differ much from the conventional thermoacoustic engines. The flow and heat transfer mechanisms of high-frequency oscillating flows is still not completely understood despite many analyses.

Numerous studies of fluid–solid conjugate heat transfer in oscillating flows have been reported. An analytical solution for small Reynolds number oscillating flow was presented by Liao et al. (1994) for fully-developed oscillating flow with heat transfer in a 2D parallel-plate channel. Bauwens (1996) proposed a closed-form approximate solution for two-dimensional oscillating flow and heat transfer in a cylindrical tube. The transverse fluid–wall conjugate heat transfer was assumed to be very effective so that the temperature and heat flux distribution were assumed to be uniform. Lu and Cheng (2000) obtained analytical solutions for the frictional factor and Nusselt number of a viscous compressible flow oscillating at high frequencies in a tube subjected to a steady cyclic axial temperature variation. They analyzed the local heat transfer rate of a compressible oscillating flow in a tube with an isothermal

* Corresponding author. Tel.: +86 10 62772919; fax: +86 10 62781610.

E-mail addresses: mfk03@mails.tsinghua.edu.cn (F. Meng), mmwang@ucdavis.edu (M. Wang), lizhx@tsinghua.edu.cn (Z. Li).

between two parallel plates with a linearized assumption. They found good agreement between the analytical and numerical solutions for both the velocities and temperatures. Thus, the LBM can effectively simulate oscillating flows and heat transfer.

Most studies have treated the thermal boundary condition as simple constant temperature or constant heat flux (D’Orazio and Succi, 2003). Few studies have used a conjugate interface thermal boundary condition. Mishra et al. (2005) used the LBM to solve the energy equation for a 2D transient conduction–radiation problem. Wang et al. (2007) simulated steady conjugate heat transfer using the LBM with a “half lattice division” treatment for the fluid–solid interaction and the energy transport, which insures temperature and heat flux continuity at the interface. This method is more appropriate for steady flow and heat transfer problems. Both Mishra et al. (2005) and Wang et al. (2007) pointed out that the LBM simulations of conjugate heat transfer converge to steady state faster than the FVM does.

This paper describes the use of the thermal LBM to simulate the conjugate heat transfer for an oscillating flow between two parallel plates. A new method is presented for treating the thermal boundary condition at the fluid–solid interface. The characteristics of the oscillating flow and heat transfer will be discussed.

2. Thermal lattice Boltzmann model

2.1. Double-species thermal lattice Boltzmann model

The lattice Boltzmann model implemented in the current investigation is the double-species lattice Boltzmann model developed by He et al. (1998). The macroscopic density and velocity evolutions are simulated by the density distribution function with the temperature evolution simulated using the internal energy distribution function.

The evolution equation for the density distribution function, \bar{f}_i , is

$$\bar{f}_i(\mathbf{r} + \mathbf{c}_i \delta t, t + \delta t) - \bar{f}_i(\mathbf{r}, t) = -\frac{\delta t}{\tau_v + 0.5 \delta t} [\bar{f}_i(\mathbf{r}, t) - f_i^{\text{eq}}(\mathbf{r}, t)], \quad (1)$$

where

$$\bar{f}_i = f_i + \frac{\delta t}{2\tau_v} (f_i - f_i^{\text{eq}}) \quad (2)$$

and τ_v is the momentum relaxation time:

$$\tau_v = \nu/RT_m. \quad (3)$$

Eq. (2) gives the transformation from f_i to \bar{f}_i . The transformation is introduced to avoid implicitness in the scheme and to evolve f_i directly.

The evolution equation for the internal energy distribution function, \bar{g}_i , is

$$\bar{g}_i(\mathbf{r} + \mathbf{c}_i \delta t, t + \delta t) - \bar{g}_i(\mathbf{r}, t) = -\frac{\delta t}{\tau_g + 0.5 \delta t} [\bar{g}_i(\mathbf{r}, t) - g_i^{\text{eq}}(\mathbf{r}, t)] - \frac{\tau_g f_i(\mathbf{r}, t) Z_i \delta t}{\tau_g + 0.5 \delta t}, \quad (4)$$

where

$$\bar{g}_i = g_i + \frac{\delta t}{2\tau_g} (g_i - g_i^{\text{eq}}) + 0.5 f_i Z_i \delta t, \quad (5)$$

Z_i represents the effect of viscous dissipation heating:

$$Z_i = (\mathbf{c}_i - \mathbf{u}) \cdot \left[\frac{\partial \mathbf{u}}{\partial t} + (\mathbf{c}_i \cdot \nabla) \mathbf{u} \right] \quad (6)$$

and τ_g is the internal energy relaxation time:

$$\tau_g = 0.5\zeta/RT_m, \quad (7)$$

where ζ represents the thermal diffusivity.

The density ρ , velocity \mathbf{u} , internal energy ε and heat flux \mathbf{q} are calculated as

$$\rho = \sum_i \bar{f}_i, \quad (8)$$

$$\rho \mathbf{u} = \sum_i \mathbf{c}_i \bar{f}_i, \quad (9)$$

$$\rho \varepsilon = \rho \frac{DRT}{2} = \sum_i \bar{g}_i - \frac{\delta t}{2} \sum_i f_i Z_i, \quad (10)$$

$$\mathbf{q} = \left(\sum_i \mathbf{c}_i \bar{g}_i - \rho \varepsilon \mathbf{u} - \frac{\delta t}{2} \sum_i \mathbf{c}_i f_i Z_i \right) \frac{\tau_g}{\tau_g + 0.5 \delta t}. \quad (11)$$

For the two-dimensional, nine-speed (D2Q9) lattice with a lattice streaming speed $c = \sqrt{3RT_m}$, as shown in Fig. 1, where T_m is the average temperature, the lattice velocities in the nine directions are

$$\mathbf{c}_i = \begin{cases} 0, & i = 0, \\ c \left(\cos \left(\frac{(i-1)\pi}{2} \right), \sin \left(\frac{(i-1)\pi}{2} \right) \right), & i = 1, 2, 3, 4, \\ \sqrt{2}c \left(\cos \left[\frac{(i-5)\pi}{2} + \frac{\pi}{4} \right], \sin \left[\frac{(i-5)\pi}{2} + \frac{\pi}{4} \right] \right), & i = 5, 6, 7, 8. \end{cases} \quad (12)$$

The density equilibrium distribution, f_i^{eq} , is expressed as

$$f_i^{\text{eq}} = w_i \left[1 + \frac{3\mathbf{c}_i \cdot \mathbf{u}}{c^2} + \frac{9(\mathbf{c}_i \cdot \mathbf{u})^2}{2c^4} - \frac{3\mathbf{u} \cdot \mathbf{u}}{2c^2} \right], \quad (13)$$

where $w_0 = 4/9$ and $w_i = 1/9$ for $i = 1, 2, 3, 4$ and $w_i = 1/36$ for $i = 5, 6, 7, 8$.

The energy equilibrium distribution, g_i^{eq} , is

$$g_i^{\text{eq}} = \begin{cases} -\frac{2\rho\varepsilon}{3} \frac{\mathbf{u} \cdot \mathbf{u}}{c^2}, & i = 0, \\ \frac{\rho\varepsilon}{9} \left[1.5 + 1.5 \frac{\mathbf{c}_i \cdot \mathbf{u}}{c^2} + 4.5 \frac{(\mathbf{c}_i \cdot \mathbf{u})^2}{c^4} - 1.5 \frac{\mathbf{u} \cdot \mathbf{u}}{c^2} \right], & i = 1, 2, 3, 4, \\ \frac{\rho\varepsilon}{36} \left[3 + 6 \frac{\mathbf{c}_i \cdot \mathbf{u}}{c^2} + 4.5 \frac{(\mathbf{c}_i \cdot \mathbf{u})^2}{c^4} - 1.5 \frac{\mathbf{u} \cdot \mathbf{u}}{c^2} \right], & i = 5, 6, 7, 8. \end{cases} \quad (14)$$

He et al. (1998) recovered the correct continuity, momentum and energy equations from the Boltzmann–BGK equation by using the Chapman–Enskog expansion.

2.2. Boundary conditions

Both the pressure boundary condition implemented at the inlet and the non-slip velocity boundary conditions at the fluid–solid interfaces are treated by the method presented by Zou and He (1997). This method is based on the idea of bounce-back of the non-equilibrium density distribution function and is approximately second-order accurate.

To treat isothermal and constant heat flux boundary conditions, D’Orazio and Succi (2003) assumed a counter-slip internal energy for each unknown internal energy distribution function which is determined consistently with Dirichlet or Neumann boundary constraints. This model has the highest accuracy because it guarantees the given temperature or heat flux at the wall (Tang et al., 2005). For an isothermal wall, such as the interface shown in Fig. 1, the unknown internal energy distribution functions for the fluid are \bar{g}_2, \bar{g}_5 and \bar{g}_6 which are assumed to be

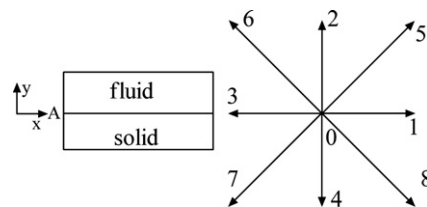


Fig. 1. Schematic of fluid–solid conjugate interface and the D2Q9 lattice.

$$\bar{g}_i = \rho(\varepsilon + \varepsilon') \text{ [corresponding form for equilibrium]}, \quad i = 2, 5, 6. \quad (15)$$

The corresponding equilibrium was given in Eq. (14). The constraint in Eq. (10) yields

$$\rho\varepsilon' = 2\rho\varepsilon + 1.5\delta t \sum_i f_i Z_i - 3G_k, \quad (16)$$

where G_k is the sum of the known internal distribution functions for the fluid at the interface

$$G_k = \bar{g}_0 + \bar{g}_1 + \bar{g}_3 + \bar{g}_4 + \bar{g}_7 + \bar{g}_8. \quad (17)$$

Once the counter-slip internal energy $\rho\varepsilon'$ is determined from Eq. (16), all the unknown distribution functions can be calculated from Eq. (15). In the case of a wall with a prescribed heat flux, the unknown internal distribution functions can be determined by the similar procedure as with the isothermal boundary.

As shown in Fig. 1, the thermal boundary condition on the fluid–solid interface is neither a Dirichlet nor a Neumann boundary condition. In the numerical simulations, neither the temperature nor the heat flux can be prescribed on the interface. The continuities of the temperature and the y -direction heat flux in the fluid and in the solid should be guaranteed at the conjugate interface. This model uses different internal energy distribution functions for the fluid and the solid, with the fluid internal distribution functions being \bar{g}_i and the solid distribution functions being \bar{g}_s^i . The evolution equation for the solid internal energy distribution function, \bar{g}_s^i , is

$$\bar{g}_s^i(\mathbf{r} + \mathbf{c}_i \delta t, t + \delta t) - \bar{g}_s^i(\mathbf{r}, t) = -\frac{\delta t}{\tau_{gs} + 0.5\delta t} [\bar{g}_s^i(\mathbf{r}, t) - g_s^{ieq}(\mathbf{r}, t)], \quad (18)$$

where τ_{gs} is the solid internal energy relaxation time. The energy equilibrium distribution, g_s^{ieq} , is

$$g_s^{ieq} = \begin{cases} 0, & i = 0, \\ \frac{\rho\varepsilon}{6}, & i = 1, 2, 3, 4, \\ \frac{\rho\varepsilon}{12}, & i = 5, 6, 7, 8. \end{cases} \quad (19)$$

As shown in Fig. 1, the fluid distribution functions, \bar{g}_2 , \bar{g}_5 and \bar{g}_6 , on the conjugate interface are unknown fluxes from the solid. The solid distribution functions, \bar{g}_s^4 , \bar{g}_s^7 and \bar{g}_s^8 , on the interface are unknown fluxes from the fluid. The treatment for the thermal boundary conditions on the conjugate interface seeks to determine these unknown internal distribution functions. The temperature and the y -direction heat flux in the fluid and in the solid are continuous at the conjugate interface:

$$\sum_i \bar{g}_i - 0.5\delta t \sum_i f_i Z_i = C_{fs} \sum_i \bar{g}_s^i, \quad (20)$$

$$\sum_i c_{iy} \bar{g}_i - 0.5\delta t \sum_i c_{iy} f_i Z_i = K_{sf} \sum_i c_{iy} \bar{g}_s^i, \quad (21)$$

where

$$C_{fs} = \frac{\rho c_{v,f}}{\rho_s c_{v,s}}, \quad (22)$$

$$K_{sf} = \frac{\tau_{gs}}{\tau_{gs} + 0.5\delta t} \frac{\tau_g + 0.5\delta t}{\tau_g}. \quad (23)$$

ρ_s is the solid density, $c_{v,f}$ is the fluid specific heat and $c_{v,s}$ is the solid specific heat.

Because of the zero velocity on the conjugate interface, \bar{g}_2 , \bar{g}_5 and \bar{g}_6 can be assumed to be

$$\bar{g}_i = \begin{cases} \frac{1}{6}\rho(\varepsilon + \varepsilon'), & i = 2, \\ \frac{1}{12}\rho(\varepsilon + \varepsilon'), & i = 5, 6 \end{cases} \quad (24)$$

and \bar{g}_s^4 , \bar{g}_s^7 and \bar{g}_s^8 for the solid are

$$\bar{g}_s^i = \begin{cases} \frac{1}{6}\rho_s(\varepsilon_s + \varepsilon'_s), & i = 4, \\ \frac{1}{12}\rho_s(\varepsilon_s + \varepsilon'_s), & i = 7, 8. \end{cases} \quad (25)$$

Eqs. (20)–(25) form a close system with the solid counter-slip internal energy parameter $\rho_s(\varepsilon_s + \varepsilon'_s)$ determined explicitly as

$$\rho_s(\varepsilon_s + \varepsilon'_s) = \frac{3}{K_{sf} + C_{fs}} \left[K_{sf}(\bar{g}_s^2 + \bar{g}_s^5 + \bar{g}_s^6) + \bar{g}_4 + \bar{g}_7 + \bar{g}_8 + 0.5\delta t \sum_i \frac{c_{iy}}{c} f_i Z_i - C_{fs} G_s + G_f - 0.5\delta t \sum_i f_i Z_i \right], \quad (26)$$

where G_f and G_s are the sum of the known internal energy distribution functions for the fluid and the solid on the conjugate interface:

$$G_f = \bar{g}_0 + \bar{g}_1 + \bar{g}_3 + \bar{g}_4 + \bar{g}_7 + \bar{g}_8, \quad (27)$$

$$G_s = \bar{g}_s^0 + \bar{g}_s^1 + \bar{g}_s^2 + \bar{g}_s^3 + \bar{g}_s^5 + \bar{g}_s^6. \quad (28)$$

After $\rho_s(\varepsilon_s + \varepsilon'_s)$ is determined, the fluid counter-slip internal energy parameter $\rho(\varepsilon + \varepsilon')$ can be expressed as

$$\rho(\varepsilon + \varepsilon') = C_{fs}\rho_s(\varepsilon_s + \varepsilon'_s) + 3 \left(C_{fs} G_s - G_f + 0.5\delta t \sum_i f_i Z_i \right). \quad (29)$$

Substituting Eq. (26) into Eq. (25) and Eq. (29) into Eq. (24), respectively gives all the unknown internal energy distribution functions for the fluid and the solid on the conjugate interface.

Finally, the corners of fluid–solid conjugate interface can be treated in a similar way with the counter-slip procedure imposed on each of the five unknown distribution functions for the fluid and the solid. For example, at corner A shown in Fig. 1, \bar{g}_1 , \bar{g}_2 , \bar{g}_5 , \bar{g}_6 and \bar{g}_8 for the fluid are unknown and \bar{g}_s^1 , \bar{g}_s^4 , \bar{g}_s^5 , \bar{g}_s^7 and \bar{g}_s^8 for the solid are unknown. The unknown distribution functions can be determined by the constraints of the continuities of the temperature and heat flux on the fluid–solid interface.

3. Physical model

The two-dimensional geometry is shown in Fig. 2. A viscous, compressible fluid with density, ρ , specific heat, $c_{v,f}$, dynamic viscosity, μ_f , and thermal conductivity, k_f , oscillates between two flat plates. The outer surface, Γ_3 , of upper plate which has a thickness, h_2 , is maintained at a constant temperature, T_{w2} . The outer surface, Γ_7 , of the bottom plate which has a thickness, h_1 , is maintained at a constant temperature, T_{w1} . The channel width is h and the length is L . The total height is H . The upper plate has density ρ_{s2} , specific heat $c_{v,s2}$ and thermal conductivity k_{s2} . The properties of the bottom plate are: density ρ_{s1} , specific heat ratio $c_{v,s1}$ and thermal conductivity k_{s1} . The periodic oscillating pressure condition at boundary Γ_1 is implemented as

$$p = p_m + p_1 \sin \omega t = p_m + p_1 \sin \frac{2\pi t}{\tau}, \quad (30)$$

where ω is the oscillation angular frequency and τ is the oscillation period. p_1 is the oscillation pressure amplitude, which is assumed to

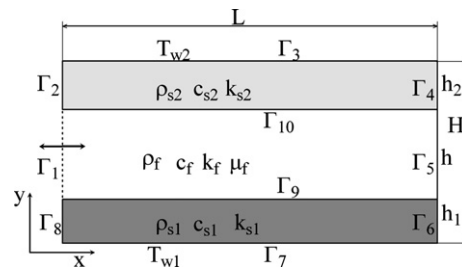


Fig. 2. Schematic of the geometry.

be small compared with the average pressure p_m in the current simulations. Non-slip velocity boundary conditions are imposed on boundaries Γ_5 , Γ_9 and Γ_{10} . Boundaries Γ_1 , Γ_2 , Γ_4 , Γ_5 , Γ_6 and Γ_8 are adiabatic. The thermal boundary conditions on Γ_9 and Γ_{10} , the fluid–solid conjugate interfaces, are treated by the model described in Section 2.

4. Results and discussion

The simulation parameters were $T_{w1} = 388$ K, $T_{w2} = 288$ K, $T_m = 313$ K, average fluid density $\rho_m = 1$ kg/m³, $\rho_m c_{v,f} = \rho_{s1} c_{v,s1} = \rho_{s2} c_{v,s2}$, gas constant $R = 286.69$ J/kg K, fluid dynamic viscosity $\mu_f = 19.1 \times 10^{-5}$ kg/(m s), average pressure $p_m = 89734$ Pa. p_1 , k_f , k_{s1} , k_{s2} , h and ω were varied chosen to study the flow and heat transfer characteristics in the oscillating flow.

4.1. Velocity distribution

For oscillating flows, the viscous penetration depth is defined as

$$\delta_\mu = \sqrt{2\nu/\omega} \tag{31}$$

The Stokes number, Λ , which is used to characterize the dominant features of the oscillating flow, is the ratio of the channel half-width to the viscous penetration depth:

$$\Lambda = h/2\delta_\mu \tag{32}$$

Fig. 3 shows the velocity distribution at cross section $x = 0.9$ L at different times in one period for $\Lambda = 8.317$. In the simulation, $\omega/2\pi = 30$ kHz. The ratio of the pressure oscillation amplitude to the average pressure, p_1/p_m , is 0.01. As shown in Fig. 3b, the y -direction velocity, u_y , also oscillates. u_y is far less than u_x . As shown in Fig. 3a, the maximum u_x across the channel at various times occurs not at the channel center, but near the walls, which is usually called the velocity “annular effect”. A similar y -direction velocity “annular effect” also exists in the large Λ case, as shown in Fig. 3b. The “annular effect” results from the viscous stresses near the walls and the periodic flow oscillations. The flow near the center of the channel

is slug-like for large Λ . When Λ is less than 1, the u_x profile is almost parabolic and the “annular effect” is not obvious. There is a standing wave node locating at the channel centerline for u_y , where the velocity does not vary, as shown in Fig. 3b. The profiles of u_y in some cross sections are anti-symmetric around the standing wave node. u_y at the two zygomorphic points around the standing wave node always have the same magnitude and opposite directions.

4.2. Temperature distribution

Fig. 4 shows the temperature distributions across the cross section $x = 0.6$ L at various times during one period. The simulation parameters are: $p_1/p_m = 0.05$, $\Lambda = 3.326$, $\omega/2\pi = 30$ kHz, $k_{s1}/k_f = 0.2$ and $k_{s2}/k_f = 1.6$. Both the plate and the fluid temperatures oscillate with the same period as that of the velocity. The temperature continuity of the fluid and the plates can be seen to be continuous at the fluid–solid interfaces, which validates the treatment of the conjugate interface condition. As shown in Fig. 7, the temperature oscillations in the two plates and the fluid are very large with obvious temperature oscillations in the plates and the fluid. The temperature oscillations in the two plates are always less than that in the fluid regardless of whether the two plates thermal conductivities are larger than that of the fluid, as shown in Fig. 4. The temperature oscillations in the two plates are a function of the plates’ thermal conductivities. As shown in Fig. 4, the temperature oscillations in the upper plate with $k_{s2}/k_f = 1.6$ are larger than those in the bottom plate with $k_{s1}/k_f = 0.2$. Obvious temperature oscillations can be observed in the upper plate but not in the lower one. The results show that the large plate thermal conductivity improves the thermal diffusion.

An interesting phenomena observed in Fig. 4 is that the lowest temperature in the bottom plate takes place not at the fluid–solid interface but in the plate interior, such as at $t = 1.375\tau$. This phenomenon is caused by the large fluid temperature oscillations and the small bottom plate thermal conductivity. In this case, the fluid temperature oscillations are so large that the fluid temperature can be higher than the bottom plate temperature near the bottom conjugate interface. The small bottom plate thermal conductivity reduces the thermal diffusion in the plate, so the lowest temperature may occur inside the plate. With these phenomena, heat will be transferred from the fluid to the bottom plate even though it has a higher outer surface temperature. This phenomena does not occur with small p_1/p_m oscillations where the fluid temperature oscillates within a narrow range and is never higher than that of the bottom plate.

4.3. Heat flux distribution

Fig. 5 shows the y -direction heat flux, q_y , distribution across the cross section $x = 0.6$ L at various times during one period. The con-

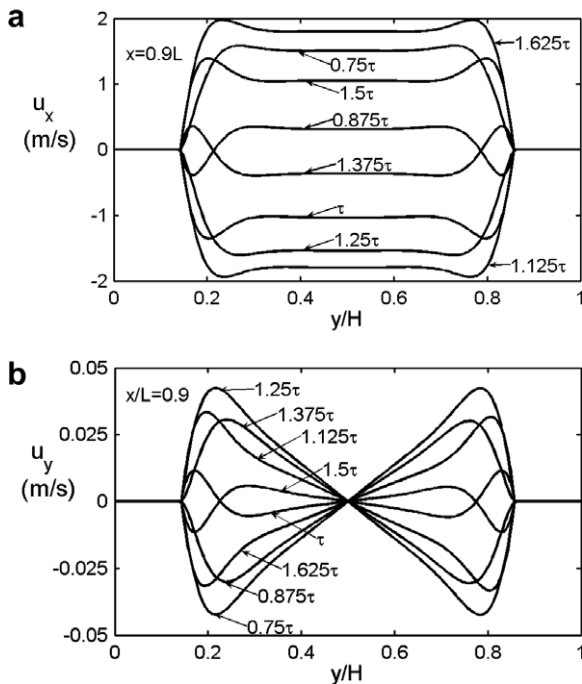


Fig. 3. x -direction (a) and y -direction (b) velocity distributions across a cross section $x = 0.9$ L at various times during one period ($p_1/p_m = 0.01$, $\Lambda = 8.317$).

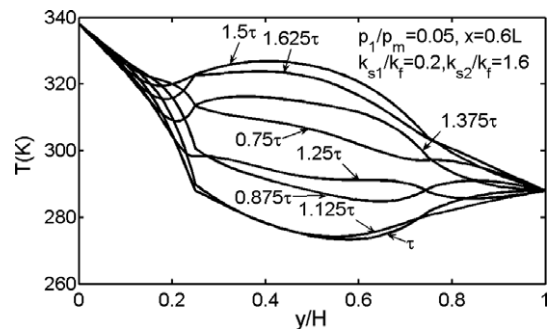


Fig. 4. Temperature distributions across a cross section $x = 0.6$ L at various times during one period ($p_1/p_m = 0.05$, $\Lambda = 3.326$).

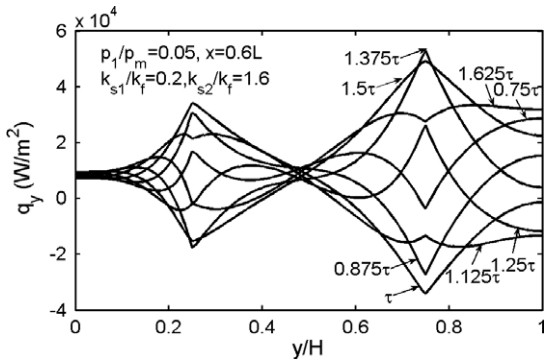


Fig. 5. y -direction heat flux distributions across a cross section $x = 0.6 L$ at various times during one period ($p_1/p_m = 0.05$, $\Lambda = 3.326$).

dition in Fig. 5 corresponds to that in Fig. 4. q_y oscillates with the same period as the temperature. The distribution of q_y of in the fluid and the plates is continuous at the fluid–solid conjugate interfaces, which validates the method used for the fluid–solid interface. The oscillations of q_y vary across the cross section. Regardless of whether the plate thermal conductivity is larger than that of the fluid, the oscillations of q_y at the conjugate interface are higher than those in the plate and in the fluid near the conjugate interface, as shown in Fig. 5. The q_y oscillation in the fluid is very small and nearly constant near the channel centerline. When p_1/p_m is large, as shown in Fig. 5 ($p_1/p_m = 0.05$), q_y is negative at times so heat flows from the fluid to the bottom plate at times as mentioned in the previous section. When p_1/p_m is small, such as $p_1/p_m = 0.01$, q_y is always positive and the heat always flows from the high temperature bottom plate to the upper plate. The average q_y over one period is always positive for both values of p_1/p_m .

4.4. Heat transfer enhancement discussion

The time and space averaged y -direction heat flux, $q_{y,ave}$, on the outer surface of the upper plate is defined as

$$q_{y,ave} = \frac{1}{\tau L} \int_{t_0}^{t_0+\tau} \int_0^L q_y(x, H, t) dx dt. \tag{33}$$

When the fluid is not moving and both the left and right sides are adiabatic, the y -direction heat flux, $q_{y,cond}$, is the same as for pure heat conduction. The ratio of $q_{y,ave}$ to the corresponding $q_{y,cond}$ represents the average heat transfer enhancement due to the oscillating flow relative to pure heat conduction. Fig. 6 shows how $q_{y,ave}$ and $q_{y,ave}/q_{y,cond}$ vary with p_1/p_m for p_1/p_m from 0.005 to 0.07 and an oscillation frequency of 30 kHz. Both $q_{y,ave}$ and $q_{y,ave}/q_{y,cond}$ de-

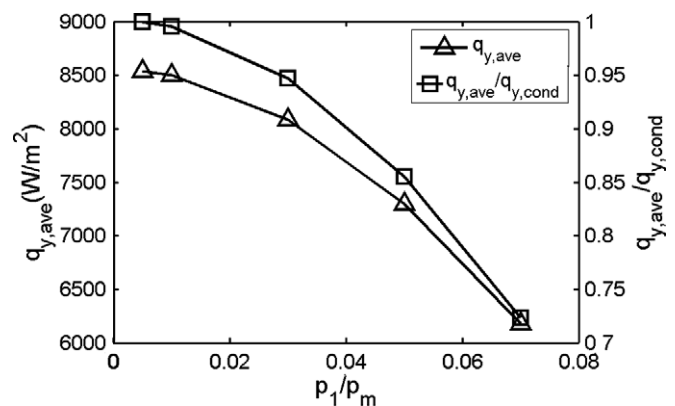


Fig. 6. $q_{y,ave}$ and $q_{y,ave}/q_{y,cond}$ for various p_1/p_m ($\Lambda = 3.326$, $k_{s1}/k_f = 0.2$, $k_{s2}/k_f = 1.6$).

crease as p_1/p_m increases. When p_1/p_m is small, such as for $p_1/p_m = 0.005$ in Fig. 6, $q_{y,ave}/q_{y,cond}$ is about 1, which means that the average heat transfer is about the same as that of pure heat conduction. For large p_1/p_m , $q_{y,ave}/q_{y,cond}$ is less than 1, which means that the oscillating flow does not enhance the heat transfer. The fluid compressibility reduces the heat transfer when the temperature are linear so the average heat transfer resistance increases with increasing p_1/p_m .

The effect of frequency influence on the average heat transfer was investigated for various frequencies for the oscillating flow between two one-wavelength long flat plates. Some simulation parameters were: $p_1/p_m = 0.01$, $k_{s1}/k_f = 1/12$, $k_{s2}/k_f = 1/2$ and $h_1 = h_2 = 0.2 h$. The two plates length, L , were adjusted to be equal to one wavelength for the various oscillation frequencies. $q_{y,ave}/q_{y,cond}$ is plotted versus the oscillation frequency in Fig. 7 for frequencies from 20 to 900 kHz. The result shows that $q_{y,ave}/q_{y,cond}$ increases linearly with the frequency. The result agrees well with the analytical result of Vainshtein et al. (1995). For the relatively low-frequency cases with frequency less than 100 kHz, $q_{y,ave}/q_{y,cond}$ is 1 approximately so low-frequency oscillating flows do not enhance the heat transfer. For the higher frequency cases, $q_{y,ave}/q_{y,cond}$ is larger than 1 and increases rapidly with frequency. The high-frequency oscillating flow markedly enhances the heat transfer. For example, $q_{y,ave}$ for 900 kHz is about 30% higher than $q_{y,cond}$.

The heat transfer enhancement is due to nonlinear acoustic streaming in high-frequency flows which is a non-zero time-averaged velocity. The formation of acoustic streaming structures results from the interaction between the wave field and the viscous boundary. In low-frequency flows, the perfectly sinusoidal profile of flow velocity is weakly distorted due to viscous and nonlinear effects. The periodically averaged flow velocity is almost zero in low-frequency flows and acoustic streaming cannot formed. In the high-frequency flow, the mean flow field during one period is shown in Fig. 8. The simulation parameters are: $\omega/2\pi = 24$ kHz, $p_1/p_m = 0.01$, $k_{s1}/k_f = 1/12$, $k_{s2}/k_f = 1/6$ and $\Lambda = 14.67$. Six vortices exist in the flow field. Three acoustic streaming circulations are clockwise and the other three circulations are counter-clockwise. The similar flow patterns have been reported by Haydock and Yeomans (2001) and Aktas and Farouk (2004). Acoustic streaming introduces an additional convective heat transfer mode into the system, so the heat transfer can be enhanced.

The enhancement due to acoustic streaming increases with the acoustic streaming velocity. The periodically averaged acoustic streaming velocity in the x -direction can be defined as

$$u_{ave} = \frac{\sum_{t=0}^{\tau} \sum_{N_h} \sum_{N_t} |u(x, y, t)|}{\tau N_h N_L}, \tag{34}$$

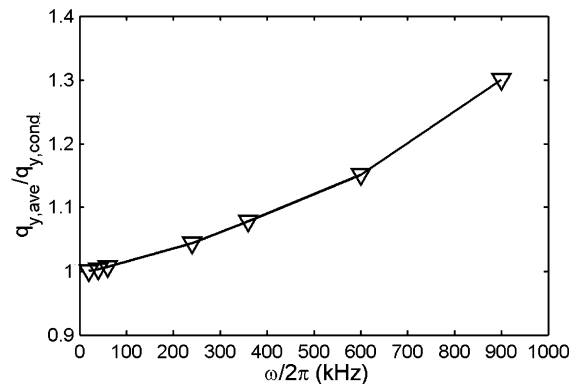


Fig. 7. $q_{y,ave}/q_{y,cond}$ for various frequencies ($p_1/p_m = 0.01$, $k_{s1}/k_f = 1/12$, $k_{s2}/k_f = 1/2$).

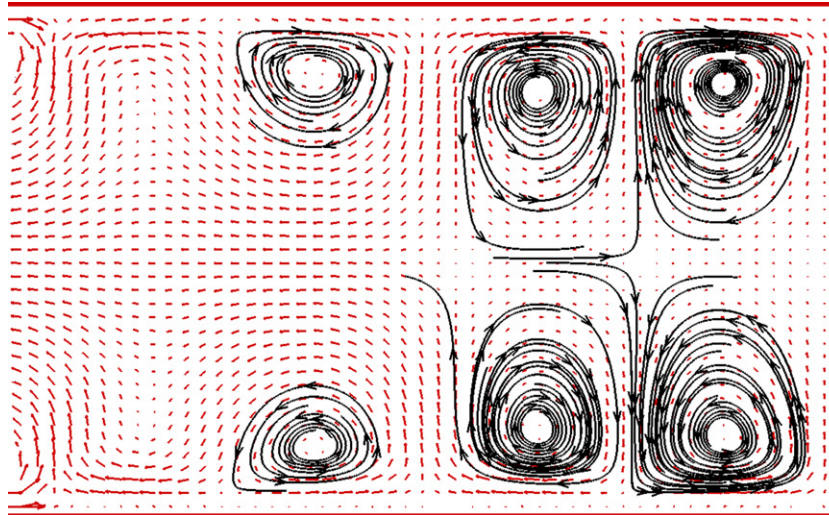


Fig. 8. Mean flow field during the 100th period in the channel.

where N_L and N_h are the node numbers in x - and y -directions. The u_{ave} for various oscillation frequencies plotted in Fig. 9 show that the averaged acoustic streaming velocity increases with frequency. While the oscillating frequency is relatively low, the average acoustic streaming velocity is too small to markedly influence on heat transfer while higher u_{ave} markedly enhance the heat transfer.

$q_{y,ave}$ and $q_{y,ave}/q_{y,cond}$ are listed in Table 1 for different plate and fluid thermal conductivities. The simulation parameters were: $p_1/p_m = 0.01$, $\omega/2\pi = 30$ kHz and $h_1 = h_2 = 0.375$ h. The results show that $q_{y,ave}$ is mainly determined by the fluid thermal conductivity. When the fluid thermal conductivity is large, such as in cases 3, 5 and 6, $q_{y,ave}$ is much larger than for the other cases. Case 3 represents the case when k_{s1} is large and k_{s2} is small. Case 6 represents the reverse case that the k_{s1} is small and k_{s2} is large. The fluid thermal conductivity is the same in both cases. $q_{y,ave}$ in the two cases are nearly the same, which means that exchanging the plate ther-

mal conductivities has no influence on $q_{y,ave}$. This characteristic can also be understood by comparing case 2 and case 4. Although $q_{y,ave}$ varies with k_{s1}/k_f and k_{s2}/k_f markedly, $q_{y,ave}/q_{y,cond}$ changes very little from 0.966 to 1.001. $q_{y,ave}$ in the oscillating flow is not a function of k_{s1}/k_f and k_{s2}/k_f which indicates that the oscillating flow has little effect on the heat transfer.

5. Conclusions

The thermal lattice Boltzmann method (LBM) was used to simulate the conjugate heat transfer in high-frequency oscillating flows between two plates with different outer surface temperatures. A method was developed to accurately treat the conjugate thermal boundary condition on the fluid–solid interface in the thermal LBM simulations. The simulation results show that both the temperature and heat flux distributions are continuous at the interface.

The velocity, temperature and y -direction heat flux distribution characteristics were analyzed for the high-frequency flow oscillations. The velocity, temperature and heat flux distributions are oscillating with the same period. The y -direction velocity distribution profile across each cross section was anti-symmetric about a standing wave point. With large p_1/p_m oscillations, the fluid temperature may sometimes be higher than that of the high temperature bottom plate.

For $\omega/2\pi < 100$ kHz and $p_1/p_m \leq 0.01$, the oscillations were linear and the average y -direction heat flux for one period was nearly equal to that for pure heat conduction. $q_{y,ave}/q_{y,cond}$ was less than 1 for large p_1/p_m oscillations with $\omega/2\pi = 30$ kHz and decreased as p_1/p_m increased because the fluid compression increased the heat transfer resistance. The plate and fluid thermal conductivities had no influence on $q_{y,ave}/q_{y,cond}$ which was about 1 for oscillations with $\omega/2\pi = 30$ kHz and $p_1/p_m \leq 0.01$. For high-frequency oscillations, the heat transfer was enhanced by nonlinear acoustic streaming. $q_{y,ave}/q_{y,cond}$ was greater than 1 and rapidly increased with the frequency, which means that marked heat transfer enhancement can be achieved with high-frequency oscillations. For example, $q_{y,ave}$ increased by about 30% for oscillations with $\omega/2\pi = 900$ kHz.

Acknowledgement

The present work is financially supported by National Basic Research Program of China (Grant No. 2007CB206901).

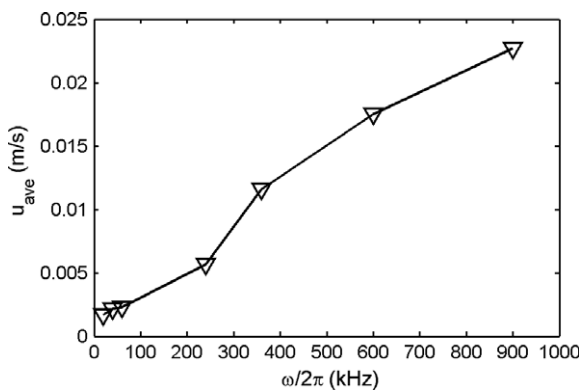


Fig. 9. u_{ave} for various frequencies ($p_1/p_m = 0.01$, $k_{s1}/k_f = 1/12$, $k_{s2}/k_f = 1/2$).

Table 1
 $q_{y,ave}$ and $q_{y,ave}/q_{y,cond}$ for various k_{s1}/k_f and k_{s2}/k_f ($p_1/p_m = 0.01$)

Case	k_{s1}/k_f	k_{s2}/k_f	$q_{y,ave}$ (W/m ²)	$q_{y,ave}/q_{y,cond}$
1	1	1	2730.4	0.978
2	20	10	2236.9	0.968
3	2	0.1	4930.8	0.998
4	10	20	2230.5	0.966
5	0.05	0.5	5320.1	1.001
6	0.1	2	4934.2	0.998

References

- Aktas, M.K., Farouk, B., 2004. Numerical simulation of acoustic streaming generated by finite-amplitude resonant oscillations in an enclosure. *Journal of the Acoustical Society of America* 116 (5), 2822–2831.
- Aktas, M.K., Farouk, B., Li, Y.Q., 2005. Heat transfer enhancement by acoustic streaming in an enclosure. *Journal of Heat Transfer* 127 (12), 1313–1321.
- Artoli, A.M., Hoekstra, A.G., Sloot, P.M.A., 2002. 3D pulsatile flow with the lattice Boltzmann BGK method. *International Journal of Modern Physics C* 13 (8), 1119–1134.
- Artoli, A.M., Hoekstra, A.G., Sloot, P.M.A., 2006. Optimizing lattice Boltzmann simulations for unsteady flows. *Computers and Fluids* 35 (2), 227–240.
- Backhaus, S., Swift, G.W., 1999. A thermoacoustic Stirling heat engine. *Nature* 399, 335–338.
- Bauwens, L., 1996. Oscillating flow of a heat-conducting fluid in a narrow tube. *Journal of Fluid Mechanics* 324, 135–161.
- Bouvier, P., Stouffs, P., Bardon, J.P., 2005. Experimental study of heat transfer in oscillating flow. *International Journal of Heat and Mass Transfer* 48 (12), 2473–2482.
- Chen, S.Y., Doolen, G.D., 1998. Lattice Boltzmann for fluid flows. *Annual Review of Fluid Mechanics* 30, 329–364.
- Chen, R.L., Chen, Y.C., Chen, C.L., Tsai, C., DeNatale, J., 2002. Development of miniature thermoacoustic refrigerators. In: 40th AIAA Aerospace Sciences Meeting and Exhibit, AIAA 2002-0206.
- Cooper, W.L., Nee, V.W., Yang, K.T., 1993. Fluid mechanics of oscillatory and modulated flows and associated applications in heat and mass transfer – a review. *Journal of Energy, Heat and Mass Transfer* 15 (1), 1–19.
- Cosgrove, J.A., Buick, J.M., Tonge, S.J., Munro, C.G., Greated, C.A., Campbell, D.M., 2003. Application of the lattice Boltzmann method to transition in oscillatory channel flow. *Journal of Physics A: Mathematical and General* 36 (10), 2609–2620.
- D'Orazio, A., Succi, S., 2003. Boundary conditions for thermal lattice Boltzmann simulations. *Lecture Notes in Computer Science* 2657, 977–986.
- Fedorov, A.G., Viskanta, R., 2000. Three-dimensional conjugate heat transfer in the microchannel heat sink for electronic packaging. *International Journal of Heat and Mass Transfer* 43 (3), 399–415.
- Guo, Z.L., Zheng, Z.G., Shi, B.C., Zhao, T.S., 2007. Thermal lattice Boltzmann equation for low Mach number flows: decoupling model. *Physical Review E* 75, 036704.
- Haydock, D., Yeomans, J.M., 2001. Lattice Boltzmann simulations of acoustic streaming. *Journal of Physics A: Mathematical and General* 34 (1), 5201–5213.
- He, X.Y., Chen, S.Y., Doolen, G.D., 1998. A novel thermal model for the lattice Boltzmann method in incompressible limit. *Journal of Computational Physics* 146 (1), 282–300.
- Herman, C., Kang, E., 2001. Experimental visualization of temperature fields and study of heat transfer enhancement in oscillatory flow in a grooved channel. *Heat and Mass Transfer* 37 (1), 87–99.
- Horvat, A., Catton, I., 2003. Numerical technique for modeling conjugate heat transfer in an electronic device heat sink. *International Journal of Heat and Mass Transfer* 46 (12), 2155–2168.
- Iwai, H., Mambo, T., Yamamoto, N., Suzuki, K., 2004. Laminar convective heat transfer from a circular cylinder exposed to a low frequency zero-mean velocity oscillating flow. *International Journal of Heat and Mass Transfer* 47 (21), 4659–4672.
- Li, P., Yang, K.T., 2000. Mechanisms for the heat transfer enhancement in zero-mean oscillatory flows in short channels. *International Journal of Heat and Mass Transfer* 43 (19), 3551–3566.
- Li, J., Peterson, G.P., Cheng, P., 2004. Three-dimensional analysis of heat transfer in a micro-heat sink with single phase flow. *International Journal of Heat and Mass Transfer* 47 (19–20), 4215–4231.
- Liao, Q.D., Yang, K.T., Nee, V.W., 1994. An analysis of conjugate heat transfer from a heated wall in a channel with zero-mean oscillatory flow for small oscillatory flow Reynolds numbers. *International Journal of Heat and Mass Transfer* 37 (Suppl. 1), 415–423.
- Liao, Q.D., Yang, K.T., Nee, V.W., 1995. Enhanced microprocessor chip cooling by channelled zero-mean oscillatory air flow. *Advances in Electronic Packaging* 2, 789–794.
- Lu, G.Q., Cheng, P., 2000. Friction factor and Nusselt number for thermoacoustic transport phenomena in a tube. *Journal of Thermophysics and Heat Transfer* 14 (4), 566–573.
- Lu, G.Q., Cheng, P., 2002. An analysis of the refrigeration mechanism of a compressible flow oscillating in a tube. *Advances in Cryogenic Engineering: Proceedings of the Cryogenic Engineering Conference* 613, 791–799.
- Mazur, Z., Hernandez-Rossette, A., Garcia-Illescas, R., Luna-Ramirez, A., 2006. Analysis of conjugate heat transfer of a gas turbine first stage nozzle. *Applied Thermal Engineering* 26 (16), 1796–1806.
- Meng, F.K., Wang, M.R., Li, Z.X., 2006. Lattice Boltzmann simulations of oscillating flow and heat transfer under linearization assumption. In: *Proceeding of the First International Conference on Enhancement and Promotion of Computational Methods in Engineering Science and Mechanics, China*, pp. 474–478.
- Mishra, S.C., Lankadasu, A., Beronov, K.N., 2005. Application of the lattice Boltzmann method for solving the energy equation of a 2-D transient conduction–radiation problem. *International Journal of Heat and Mass Transfer* 48 (17), 3648–3659.
- Nika, P., Bailly, Y., Guermeur, F., 2005. Thermoacoustics and related oscillatory heat and fluid flows in micro heat exchangers. *International Journal of Heat and Mass Transfer* 48 (18), 3773–3792.
- Qiu, S.G., Simon, T.W., 1994. Measurements of heat transfer and fluid mechanics within an oscillatory flow in a pipe. *Fundamentals of Heat Transfer in Forced Convection*, HTD 285. ASME, New York, pp. 1–7.
- Sert, C., Beskok, A., 2003. Numerical simulation of reciprocating flow forced convection in two-dimensional channels. *Journal of Heat Transfer* 125 (3), 403–412.
- Shi, Y., Zhao, T.S., Guo, Z.L., 2004. Thermal lattice Bhatnagar–Gross–Krook model for flows with viscous heat dissipation in the incompressible limit. *Physical Review E* 70, 066310.
- Swift, G.W., 1988. Thermoacoustic engines. *Journal of the Acoustical Society of America* 84 (4), 1145–1180.
- Symko, O.G., Abdel-Rahman, E., Kwon, Y.S., Emmi, M., Behunin, M.R., 2004. Design and development of high-frequency thermoacoustic engines for thermal management in microelectronics. *Microelectronics Journal* 35 (2), 185–191.
- Tang, G.H., He, Y.L., Tao, W.Q., 2005. Thermal boundary condition for the thermal lattice Boltzmann equation. *Physical Review E* 72 (1), 016703.
- Vainshtein, P., Fichman, M., Gutfinger, C., 1995. Acoustic enhancement of heat transfer between two parallel plates. *International Journal of Heat and Mass Transfer* 38 (10), 1893–1899.
- Walsh, T.E., Yang, K.T., Nee, V.W., Liao, Q.D., 1993. Forced convection cooling in microelectronic cabinets via oscillatory flow techniques. In: *World Conference on Experimental Heat Transfer, Fluid Mechanics and Thermodynamics*. Elsevier, Amsterdam, pp. 641–648.
- Wang, J.K., Wang, M.R., Li, Z.X., 2007. A lattice Boltzmann algorithm for fluid–solid conjugate heat transfer. *International Journal of Thermal Science* 46 (3), 228–234.
- Yang, S.J., 2003. Numerical study of heat transfer enhancement in a channel flow using an oscillating vortex generator. *Heat and Mass Transfer* 39 (3), 257–265.
- Zhao, T.S., Cheng, P., 1995. A numerical-solution of laminar forced-convection in a heated pipe subjected to a reciprocating flow. *International Journal of Heat and Mass Transfer* 38 (16), 3011–3022.
- Zhao, T.S., Cheng, P., 1996. Oscillatory heat transfer in a pipe subjected to a periodically reciprocating flow. *Journal of Heat Transfer* 118 (3), 592–597.
- Zou, Q.S., He, X.Y., 1997. On pressure and velocity boundary conditions for the lattice Boltzmann BGK model. *Physics of Fluids* 9 (6), 1591–1598.